PCCP

Accepted Manuscript




ROYAL SOCIETY OF CHEMISTRY

www.rsc.org/pccp

# Effect of doping $\beta$-NiOOH with Co on the catalytic oxidation of water: DFT+U Calculations†

**Francesca Costanzo,**[*a]

Electrocatalytic water splitting using energy from sunlight represents a promising strategy for clean, low-cost, and environmentally friendly production of $H_2$. Unfortunately, the oxygen evolution reaction (OER) at the anode is kinetically slow and represents the bottleneck of this process. Transition metal oxides are good candidates for the anode in electrochemical water splitting. Inspired by recent computational work on $\beta$-NiOOH, which is considered the active phase during the charging and discharging process in alkaline batteries, we performed density functional theory calculations with the inclusion of the Hubbard-U correction on selected surfaces of pure and Co-doped $\beta$-NiOOH to calculate the energetics of the OER. The goal of the paper is to investigate theoretically whether doping a NiOOH surface with Co might change the mechanism and lower the overpotential of the OER on a specific NiOOH surface, and to what extent the choice of the surface unit cell may affect the results. Our results indicate that the most likely reaction mechanism depends on the amount of Co doping. We find that doping the $\beta$-NiOOH surface with only 25% Co decreases the overpotential from 0.28 to 0.18 V. We also find that the theoretical overpotential, and which step is the potential limiting step, depends on the size of the surface unit cell selected in the calculations. This work highlights how optimizing the binding energies of the various intermediates (O, OH and $H_2O$) on the Ni and Co surface sites, may be key to reducing the overpotential.

## 1 Introduction

In the past decades, there has been considerable interest in the electrolysis of water in electrochemical cells. This process results in oxygen evolution at the anode and hydrogen evolution at the cathode, providing hydrogen as a clean and sustainable carrier of solar energy[1]. Unfortunately, the oxygen evolution reaction (OER) $2\ H_2O \rightarrow 4\ H^+ + O_2 + 4\ e^-$ (in acidic media) or $4\ OH^- \rightarrow 2\ H_2O + O_2 + 4\ e^-$ (in basic media) is kinetically slow, so that it is associated with energy loss and it currently represents the bottleneck in (photo)-electrochemical water splitting. It is therefore important to find a more efficient oxygen-evolving electrocatalyst in order to minimize the energy loss. The reason why the OER is problematic is that it involves four one-electron transfer steps, which on most materials are related to each other through scaling relationships, making it difficult to reduce the overpotential for the rate limiting step without introducing an overpotential for another step[2–4]. Efforts to improve the efficiency of OER catalysts[5–10] are focused on understanding the mechanism of the oxidation of water on oxide surfaces and lowering the overpotential associated with the rate limiting step. Current OER catalysts contain often precious metals[11], e.g. Ir and Ru, which are not suitable for large-scale applications. OER catalysts containing 3*d* transition metals such as Fe, Co or Ni, which are abundant elements, are therefore more convenient and can be made efficiently as recently demonstrated by Grätzel and coworkers[12].

NiOx has been used in lithium batteries[13–17], and is known for being moderately active[18–21]. In a recent theoretical study by Li and Selloni[22], the energetic profile of the OER was studied with density functional theory with added on-site Coulomb repulsion (DFT+U), for selected surfaces of pure $\beta$-NiOOH and Fe-doped-$\beta$-NiOOH. According to their results, in fair agreement with experiments[23,24], Fe-doped-$\beta$-NiOOH has a very low overpotential (the calculated value was 0.27 V), and this was the lowest computed overpotential among the surfaces considered.

As emphasized by Li and Selloni[22], the composition and the structure of the active phase of the NiOx phase under OER conditions is not well known. The Bode's diagram[25] (scheme 1 in the paper of Li and Selloni[22]) shows that, during the charging and discharging process in Ni alkaline batteries, various redox transformations can occur between $Ni(OH)_2$ and NiOOH. While Li and Selloni have argued that there is now a consensus that $\beta$-NiOOH is the active OER phase[18,19,22], others concluded that $\gamma$-type NiOOH is the more active OER phase[20,26].

[a] *Leiden Institute of Chemistry, Gorlaeus Laboratories, P.O.Box 9502, 2300 RA, Leiden, The Netherlands; Email f.costanzo@unibo.it*

Co-doped NiOx materials might also be active OER catalysts, as several recent experiments suggest[27,28]. Oshitani et al.[16] discovered that capacity stabilization of Ni electrodes, which prevents the formation of the $\gamma$-NiOOH oxidized state, can be achieved by the addition of the combination of $Cd(OH)_2$ and $Co(OH)_2$ to the $Ni(OH)_2$ crystal. The addition of only $Co(OH)_2$ leads to a lowering of the oxidation potential of the $Ni(OH)_2$[16]. In recent work, Sadiek et al.[29] discovered that the modification of glassy carbon, Pt and Au electrodes with mixed oxides of $NiO_x$ and $CoO_x$ promotes the OER when $CoO_x$ is deposited last. The composite electrode shows high catalytic activity, good stability and a reduced overpotential for the OER compared to the unmodified electrodes. In other recent work, Liu et al.[30] measured the highest specific capacitance to date for a nanostructured $Co_xNi_{1-x}(OH)_2$ composite by X-ray and scanning electron microscopy, suggesting that this type of compound holds promise as a potential electrode materials in supercapacitors. Using two different Co-based electrodes ($LiCoO_2$ and $LiCoPO_4$), they also found that the activation of the $LiCoPO_4$ electrode is related to the amorphous surface structure. Their work highlights that understanding and controlling surface reconstruction is important for electrocatalyst development[30].

Co and Ni have also recently been studied by Liao[31] et al. as additives to a photocatalyst. They found that doping a hematite ($Fe_2O_3$) surface by partially replacing Fe with Co and Ni leads to a lower overpotential allowing for a thermodynamically more favorable reaction pathway. Recently, Subbaraman et al.[32] investigated the importance of the OH-M bond strength on 3*d* transition metal hydr(oxy)oxide catalysts for the activity of the catalyst for the OER, with M = Ni, Co, Fe and Mn. They were able to correlate the oxophilicity (M-OH bond strength) with the overpotential measured for the OER using the catalyst. Finally, Bajdich et al.[33] recently investigated water oxidation on several surfaces of $\beta$-CoOOH, and the effect of doping surfaces with 25% Ni, using DFT+U calculations. They reported that the lowest overpotential is found on the (1014) surface of CoOOH, and that this can be further lowered by Ni doping. For a CoOx surface it was recently found that the activity of the high-index $01\bar{1}2$ surface shows activities that can explain the experimental findings[33,34], due to the higher reactivity of the unsaturated metal atoms in the former. The $(01\bar{1}2)$, $(10\bar{1}4)$ and other high-index surfaces have not been directly observed yet, mainly because the spectroscopic measurements have been of too low resolution so far. However, there are a number of strong indirect indications that this surface forms. For example, several theoretical studies have shown that the more stable, lower-index surfaces are practically inactive[35,36], which is in disagreement with the experiment findings[37]. Another example is the $\beta$-NiOOH surface, investigated by Li et al.[22], also showing activities for the high-index surface that are in good agreement with experimental findings[20]. Despite these interesting and sometimes promising findings, the effect of Co-doping on the activity of $\beta$-NiOOH as an OER catalyst remains controversial. For example, Trotochaud et al.[23] performed experiments on the $Ni_yCo_{1-y}O_x$ OER catalysts in the thin-film geometry to avoid confounding effects associated with high-surface area or thick film architectures. They did not find any synergistic effects between Co and Ni for the mixed oxide-catalysts films.

Inspired by these interesting and sometimes controversial results, we want to shed light on a possible synergistic effect of doping a $\beta$-NiOOH with Co for the OER. Starting from the work by Li and Selloni[22], we study the OER mechanisms of the OER on $\beta$-NiOOH and Co-doped-$\beta$-NiOOH, considering two different Co doping levels of the topmost layer of the $\beta$-NiOOH surface, i.e. replacing 25% and 50% of the Ni atoms in the layer exposed to the water, respectively. Anticipating our results, we find that, when the exposed layer of the $\beta$-NiOOH surface is doped with 25% of Co, the OER activity can improve by more than 60%.

Here, we investigate theoretically whether doping the NiOOH surface with Co changes the mechanism and lowers the overpotential of the OER on a specific NiOOH surface, and to what extent the answer to this result might be affected by the choice of the surface unit cell size in calculations. We adopt the same model of the NiOOH surface as recently chosen by Li and Selloni, which makes comparison of our results straightforward.

## 2 Method, computational details and model

### 2.1 Free energies calculations

We use the method from Nørskov and Rossmeisl[38] to compute the free energy diagrams of the OER mechanism. This method is based on the notion that the chemisorption energy of the reactants and intermediates is typically a good descriptor of the activity of the catalytic surface[39]. It also has a good accuracy over computational cost ratio and allows us to compare our results with several related studies[22,34]that are based on the same approach. In this approach, the discussion of energy barriers for the different elementary steps is restricted to the barriers that come from differences of free energies of the intermediates. Our analysis is focused on the thermochemistry of the reactions. However, it was established that the activation energy for dissociative chemisorption, depends linearly on the reaction energy[40–43]. Several DFT studies have shown that the Brønsted-Evans-Polanyi relations also hold for many surface reactions[40,44], which allows one to construct volcano curves where the fundamental parameter is the dissociative

[a] *Leiden Institute of Chemistry, Gorlaeus Laboratories, P.O.Box 9502, 2300 RA, Leiden, The Netherlands E-mail: f.costanzo@unibo.it*

chemisorption energy of the key[45] reactant species. Possible deviations from this linear dependence are not considered in our analysis at this stage, except for the insertion of the O adatom in the lattice (reaction 1.2) and for the release of the oxygen molecule (reactions 1.4 and 2.4), as reported in the Supporting Information.

The Nørskov and Rossmeisl method allows one to determine whether the intermediate one-electron transfer reaction steps are thermodynamically favorable, which is a necessary (but not sufficient) criterion for the reaction to proceed. Here, the reaction free energy of each elementary step is calculated as follows: $\Delta G_0 = \Delta E + \Delta ZPE - T\Delta S$. The reaction energy $\Delta E$ is calculated using density functional theory (DFT) augmented with the Hubbard (U) model, as further detailed in the following section. The standard hydrogen electrode (SHE) is used as a reference, so that the free energies of the proton $G[H^+]$ and the electron $G[e^-]$ in each elementary step can be replaced by half the free energy of the hydrogen molecule, $G[H_2]$, minus a contribution due to the bias of the electrode potential, U, versus the SHE (pH = 0, $p = 1$ bar, $T = 298.15$ K) as follows: $1/2G\ [H_2] - |e|U$. The free energy of the $O_2$ molecule is expressed as $G[O_2] = 4.92$ eV + 2 $G[H_2O]$ - 2 $G[H_2]$, in accordance with the OER equilibrium under standard conditions. In the Nørskov method[38] the free-energy change of the total reaction of one water molecule, $H_2O \rightarrow 1/2\ O_2 + H_2$, is fixed at the experimental value of 2.46 eV to avoid DFT calculations of the energy of $O_2$, which electronic structure is not well described by DFT methods[4,46]. Since the theoretical overpotential does not depend on pH, all the free energy results are calculated at pH = 0. We used the same values for $\Delta ZPE$, $\Delta H$ at 0 K and the change in entropy as used in Ref.22 since we used the same set of computational parameters. The $\Delta ZPE$ and $\Delta S$ are calculated using DFT calculations of vibrational frequencies and standard tables for gas-phase molecules[47].

### 2.2 DFT calculations

DFT calculations were performed at the generalized gradient approximation (GGA) PBE level[48] using the plane wave implementation[49] in the Quantum Espresso code[50].

We calculate the surface $\beta$-NiOOH($01\bar{1}5$) with seven layers starting from the bulk material, under the usual constraints that we maintain the bulk stoichiometry and do not induce a dipole moment along the slab normal. There are only two possible structures, which differ from each other by the H positions, but have very similar energies and expected surface-chemical behavior. We chose the surface closest to the setup used by Li and Selloni[22], for ease of comparison. During our analysis, we replicated periodically a seven-layer slab in $x$ and $y$ directions, to model the $\beta$-NiOOH($01\bar{1}5$)surface. A vacuum layer of $\approx$ 16Å was introduced between the slabs, which was sufficient to prevent interactions between periodic images of the slabs. This particular $\beta$-NiOOH surface shows a satisfactory convergence with respect to slab thickness and it was already shown to have a very low overpotential for the OER when one Ni atom is replaced by Fe[22]. The Brillouin-zone was sampled using the $3 \times 3 \times 1$ Monkhorst Pack type of $k$-points, ensuring the convergence of the energy to within 0.0015 eV. The atoms in all the layers of the surface were free to move during the optimization of the structures. Ultrasoft pseudopotentials were used to treat the ion cores. The configurations of the valence electrons of Co, Ni and O were ($3d^8 4s^1$), ($3d^9 4s^1$) and ($2s^2 2p^4$), respectively. Spin polarized calculations were performed in order to account for the presence of unpaired electrons in Co and Ni. Transition metal (TM) atoms, with their partially filled $d$-shells, are treated improperly using DFT functionals[51,52] based on the generalized gradient approximation (GGA). In particular, the strong Coulomb repulsion between the electrons in the $d$-shell leads to a significant 'self-interaction-error'[53]. This error is manifest in the inability of DFT to properly reproduce the bandgap of transition metal oxides. The application of GGA-DFT to the OER may also lead to large errors in the computed activity ($\eta$ and binding energies of the intermediates to the surface) of OER catalysts[52] and even to failure to predict the most favorable reaction mechamism[52]. A rather simple but efficient improvement is based on the Hubbard model[54–57]. In this approach, correlation effects in the electronic structure of the TM oxide are reintroduced as a correction (+U) to the total energy functional by including a repulsive Coulomb potential into DFT in the GGA[58]. All results presented here are obtained by GGA+U calculations. The effective $U - J$ terms, were 5.5 and 3 eV for Ni and Co, respectively. This $U$ value to the $d$ orbitals of the Ni atom results in a value for the lattice parameter for the $\beta$-NiOOH structure of 2.99 Å, in good agreement with previous studies[59]. In the case of Co, the $U$ correction to the $d$ orbital has been found to provide the best agreement with available experimental results for Co hydroxides surfaces[34]. The electronic wave function is well represented by a plane wave basis set with a cutoff energy of 476 eV ($\sim$ 35 Ry). The electron density is treated on a grid corresponding to a plane wave cutoff at 4762 eV ($\sim$ 350 Ry). A Gaussian smearing for the integration of the Brillouin-zone of 0.27 eV was used to ensure fast convergence of the self-consistent electron density. The Broydel-Fletcher-Goldfarb-Shanno (BFGS)[60] method was employed for geometry relaxations until the maximum force on the atoms was less than 0.001 Ry/bohr.

### 2.3 Models

Figure 1 shows different views of the relaxed $\beta$-NiOOH($01\bar{1}5$) surface. With the smallest unit cell employed here, the surface

exposes two $Ni_{5c}$, two $O_{3c}$ and two $O_b$ atoms per unit cell. We relaxed the computed lattice parameters to remove stress from the lattice, although this may lead to small deviations from the experimental numbers. For simplicity, throughout the article we will omit the index $(01\bar{1}5)$. We investigated different OER mechanisms on two different materials ($\beta$-NiOOH and $\beta$-NiOOH doped by Co) using two different surface unit cells for both materials. Figure 2 shows for both $\beta$-NiOOH and Co-doped-$\beta$-NiOOH the small (SC) and large (LC) unit cell considered, with coverage by a monolayer of $H_2O$. The SC has similar dimensions as the system used by Li and Selloni[22], while LC is twice as large. The cell parameters for the SC and LC were $a = 5.98$ Å, $b = 6.39$ Å and $\gamma$=76.23°, and $a = 11.96$ Å, $b = 6.39$ Å and $\gamma$=76.23°, respectively. For the doped material, the two units cells correspond to two different doping amounts by Co on the exposed layer of the surface: 50% and 25% in the SC and LC, respectively. In particular, for the surface doped at 50% Co, one of the two exposed pentacoordinated Ni atoms was replaced with Co, while for the surface doped at 25%, one out of the four Ni atoms was replaced with Co.

### 2.4 OER mechanisms modeled

To include possible cooperative effects between water molecules in the reaction mechanisms, the metal surface was microsolvated by a layer of explicit water molecules. This so-called micro-solvation is an indicator of the influence of the bulk solvent[5,22,61]. The overall reaction at the anode in acidic media is:

$2\ H_2O \rightarrow 4\ H^+ + 4\ e^- + O_2$.

To map out the OER pathway, we take a recursive trial-and-error approach, in which we investigate each 'likely' oxidation pathway by adding a solvent $H_2O$ to the surface and then removing H atoms (proton/electron pair) in a stepwise procedure until finally an $O_2$ species is produced. The two most likely mechanisms presented here, were selected since our goal of the paper is to investigate theoretically whether doping a NiOOH surface with Co might change the mechanism of the OER on this specific NiOOH surface. Our initial reaction is split in four steps, according to two possible mechanisms (path I and path II). Both of them consist of four one-electron transfer reaction steps. The suggested path I mechanism is the following:

$2\ H_2O^* + 2\ H_2O(l) \rightarrow H_2O^* + OH^* + H^+ + e^- + 2\ H_2O(l)$ (1.1)

$H_2O^* + OH^* + 2\ H_2O(l) \rightarrow 2\ H_2O^* + O^* + H^+ + e^- + H_2O(l)$ (1.2)

$2\ H_2O^* + O^* + H_2O(l) \rightarrow H_2O^* + OH^* + O^* + H^+ + e^- + H_2O(l)$ (1.3)

$H_2O^* + OH^* + O^* + H_2O(l) \rightarrow 2\ H_2O^* + O_2(g) + H^+ + e^-$. (1.4)

where asterisk (*) indicates that the species is adsorbed onto the surface. The mechanism proposed here, does not differ from the proper nucleophilic attack with the formation of *OOH proposed by Nørskov[2,3]. In fact, in their work the OH* + O* intermediate is often referred to as OOH*, even though an adsorbed OOH molecule is not always easily discerned[2,3], and it might be better to view it as closely spaced O* and OH*. Nevertheless, the formation of the superoxy (-OOH) intermediate by kinetic experiments has been proposed by Lyons et al.[18]. Optimized intermediate configurations of the OER and reaction energies of each one-electron transfer reaction steps according to path I are reported in Figure 3 and Table 1, respectively. During reaction 1.1, the first release of a proton from an adsorbed water molecule, leaves an adsorbed OH on the surface. Experimental evidence of two dehydrogenation reactions occurring during the OER mechanism has already been reported[62–64]. After the second release of a proton from the adsorbed OH, reaction 1.2, an O-O bond forms between the O adatom and a surface lattice $O_{3c}$, while a solvent water molecule adsorbs at the exposed $Ni_{5c}$ adjacent to the O-O species. We explored the effective possibility of the insertion of the O adatom into the lattice, according to reaction 1.2 and of the release of the oxygen molecule according to reactions 1.4 and 2.4. The results of these kinetic activation barriers are reported in the Supporting Information. During reaction 1.3 another adsorbed $H_2O$ loses a proton and transforms into an adsorbed OH. After the fourth proton release, reaction 1.4, $O_2$ forms and desorbs from the surface, thus allowing another solvent water molecule to adsorb on the exposed $Ni_{5c}$. In this way, the $H_2O$ monolayer adsorbed on the initial catalyst is recovered.

For clarity, we call the oxygen added to the surface during reaction 1.2 an adatom. During the second mechanism considered, path II, the reactions 1.2 and 1.3 are switched. Path II consists of two subsequent dehydrogenation reactions (reactions 2.1 and 2.2) followed by two reactions (2.3 and 2.4) where the adsorbed intermediates on the surface react with two water molecules of the solvent as follows:

$2\ H_2O^* + 2\ H_2O(l) \rightarrow H_2O^* + OH^* + H^+ + e^- + 2\ H_2O(l)$ (2.1)

$H_2O^* + OH^* + 2\ H_2O(l) \rightarrow 2\ OH^* + H^+ + e^- + 2\ H_2O(l)$ (2.2)

$2\ OH^* + 2\ H_2O(l) \rightarrow H_2O^* + OH^* + O^* + H^+ + e^- + H_2O(l)$ (2.3)

$H_2O^* + OH^* + O^* + H_2O(l) \rightarrow 2\ H_2O^* + O_2(g) + H^+ + e^-$. (2.4)

The interchange of steps 1.2 and 1.3 becomes possible once OOH* is viewed as closely spaced O* and OH* (see above). Optimized intermediate configurations involved in the OER and the energetics of each one-electron transfer reaction step according to path II are reported in Figure 4 and Table 2, respectively. We studied the OER pathways on pure $\beta$-NiOOH

and Co-doped-$\beta$-NiOOH in the SC and the LC, according to both mechanisms.

## 3 Results and discussion

### 3.1 Path I on the pure and the 50% Co doped $\beta$-NiOOH surface using the small unit cell

In the following we describe the calculated energy-pathways for the OER according to path I on the pure and the 50% Co doped $\beta$-NiOOH surfaces using the small cell (SC). The optimized intermediate configurations are shown in Figure 3 and the corresponding reaction energies are reported in Table 1. The results for the pure $\beta$-NiOOH surface agree well with previous calculations[22] and the overpotential ($\eta$) for the potential determining step (PDS) at reaction 1.1 is 0.47 V (1.70 eV - 1.23 eV/q), compared to 0.46 V in Ref.[22]. The deviation of the cumulative free energy, ($\Delta$G 1.1 + $\Delta$G 1.2 = 2.83 eV) from the ideal value (2.46 eV) to split the water is illustrated in Figure 5A.

Next, we consider the effect of doping the exposed layer of the $\beta$-NiOOH surface with 50% Co. The optimized intermediate configurations computed with the SC are shown in the second row of Figure 3, and the energies are reported in Table 1. For this surface, reaction 1.2 is the PDS, yielding an $\eta$ of 0.58 V.

The differences in the free energy profiles of these two surfaces are shown in Figure 5A and can be explained from the relative stability of the subsequent intermediates during the OER. The interaction between Co and the adsorbed OH group (OH*) is more favorable than that between Ni and OH*, in agreement with the findings of Ref.[32]. Note also that Co has one less *d*-electron than Ni, making it likely that in a situation where Co replaces Ni in NiOOH, Co will interact more favorably with the unpaired electron of OH than Ni. For Co-doped-$\beta$-NiOOH, reaction 1.1 is then rather favorable ($\Delta$G 1.1 = 1.18 eV). As also illustrated in Figure 5A, $\Delta$G 1.1 for the Co-doped-$\beta$-NiOOH is very close to the ideal value necessary to split water (1.23 eV) while $\Delta$G 1.1 for $\beta$-NiOOH is significantly larger ($\Delta$G 1.1 = 1.70 eV). With an overpotential of 0.58 V (Table 1), reaction 1.2 becomes the PDS for the Co-doped material, possibly because the adsorption of the O-adatom requires a larger deformation of the surface (see Figure 3). Figure 5A shows that for the doped surface the deviation of 0.53 eV from the ideal value (2.46 eV) of the second intermediate level for water splitting is quite significant, while for the pure surface it is negligible (2.83 eV). The high overpotential on the Co-doped surface is thus mostly a consequence of the high free energy of Config.3 of this surface (it contributes 0.53 V to the overpotential of 0.58 V), the remainder of the overpotential being due to the free energy of Config.2 being too low by 0.05 eV for the Co-doped surface.

Our analysis of the energies is supported by a comparison of the structural parameters for the optimized configurations during the OER in path I. Table 3 reports the distances between the metal ion (Co or Ni) and the oxygen of the adsorbed species for the intermediates of the pure and doped surface during the OER in path I. According to Subbaraman et al.[32], the M-O distance can be used as an indicator of the activity of the catalyst. The distance between the metal closest to the oxygen of the OH* in Config.2 is shortened by 0.07 Å for Co with respect to Ni, which is indicative of the more favorable energetic interaction of OH* with Co. Moreover, the deformation of the structure due to the adsorption of an O-adatom in the surface is somewhat larger for Co than for Ni in Config.3, with the metal-metal distance being larger for the doped material (3.25 Å for Ni-Co) than for the pure surface (3.20 Å for Ni-Ni), respectively. We therefore attribute the higher free energy level of Config.3 of the doped surface to the greater surface deformation observed for this surface. Taken together, the higher free energy level of Config.3 of the doped surface (due to its larger surface deformation) and the lower free energy level of Config.2 (due to the more favorable interaction of Co with OH*) explain why reaction 1.2 becomes the PDS for the cobalt doped surface.

Finally, a comparison of the overpotentials calculated assuming the OER mechanism to be path I and using the SC suggests that doping the NiOOH surface with Co somewhat increases the overpotential, from 0.47 to 0.58 V.

### 3.2 Path I on the 25% Co doped $\beta$-NiOOH surface using the large unit cell

Next we study the effect of lowering the amount of Co doping of the surface layer of $\beta$-NiOOH. The bottom row of Figure 3 shows the optimized configurations of 25% Co-doped-$\beta$-NiOOH using the LC. The relative energies are reported in Table 1. Similar to the 50% doped surface, the PDS for this surface is reaction 1.2 with an $\eta$ = 0.53 V. The decrease of $\eta$ from 0.58 to 0.53 V going from the 50% Co-doped to the 25% Co doped surface layer of NiOOH is a consequence of a larger decrease of the free energy of Config.3 than the decrease observed in the free energy level of Config.2. In other words, both configurations decrease in energy, but relative to Config.1 the free energy of Config.3 decreases more (by 0.23 eV) than Config.2 (by 0.18 eV) if the amount of doped Co is decreased from 50 to 25%.

We attribute the decrease of the free energy level of Config.3 to a greater capacity of the larger surface unit cell to accommodate the strain due to the presence of the O-adatom in the surface. It is not so clear why the free energy level of Config.2 is likewise decreased with decreased Co-doping. The Co-OH* distance we computed for the 25% Co doped surface is actually a bit larger (1.82 Å) than the value for the 50%

doped Co doped surface (1.80 Å, see Table 3).

The increased stability of Config.2 with the LC could be due, once again, to the less repulsive electrostatic interactions between OH* and its periodic images in the *x* and *y* directions and the better arrangement of the overlayer of the water molecules with the increased size of the surface. It is also possible that there are effects due to whether or not the $H_2O$ overlayer (or the mixed OH-$H_2O$ overlayer) is commensurate with the size of the surface unit cell[65].

### 3.3 Path II on the pure $\beta$-NiOOH surface using the small unit cell

We optimized the structures of the reactant and product species along the OER according to path II on the pure $\beta$-NiOOH surface using the SC and we found that the electronic structure of Config.3 is very difficult to converge due to the presence of two unfavorable interactions between OH and Ni. Also because the overpotential would be at least 0.47 V in any case (reaction 2.1 is still the same as reaction 1.1, which is the PDS according to path I for the small cell), these calculations were abandoned.

### 3.4 Path II on the pure and the 25% Co doped $\beta$-NiOOH surface using the large unit cell

As discussed in the previous sections, the PDS for the Co-doped surface at both the 25% and 50% doping level is reaction 1.2 in which an O-adatom is adsorbed on the surface. We have also explained why this reaction is more favorable for the pure than for the Co-doped surfaces. Starting from these considerations, we have explored the alternative path for the pure and Co-doped surfaces (see the Section 'Modeled OER mechanisms').

We explored path II only with the larger cell (LC) for both the pure and the 25% doped $\beta$-NiOOH surface. The optimized structures of the OER intermediates and their reaction free energies are reported in Figure 4 and Table 2, respectively; the free energy profile is shown in Figure 5B.

On the Co-doped-$\beta$-NiOOH surface, during reaction 2.1, the first proton is released by a water molecule that is adsorbed on the exposed Co. In reaction 2.2, a water molecule that is adsorbed on the exposed $Ni_{5c}$ that is adjacent to the OH* adsorbed on Co, also donates a proton to the solvent and transforms into a second OH*. After the release of a third proton from the OH* on the exposed $Ni_{5c}$ atom in reaction 2.3, an O-O bond forms between the O adatom and a surface lattice $O_{3c}$, while a new solvent water molecule adsorbs on the exposed $Ni_{5c}$ adjacent to the O-O species. In the final reaction, 2.4, the fourth proton is released from the OH* adsorbed on Co, and $O_2$ desorbs from the surface followed by the adsorption of another water molecule on the vacated Co to recover the initial state of the catalyst.

The free energy profile in Figure 5B shows that reaction 2.1 is thermodynamically favorable, as found earlier for path I. In path II, reaction 2.2 is the PDS and the calculated overpotential is only 0.18 V ((1.41 eV - 1.23 eV)/q). The free energy profile shows that the free energy level of Config.3 ($\Delta$G 2.1 + $\Delta$G 2.2 = 2.41 eV) is very close to the ideal value (2.46 eV) for splitting water. Indeed, in path II reaction 2.2 involves the adsorption of OH* and not an adsorption of the oxygen adatom in the surface, as in the case in reaction 1.2 in path I. In Config.3 a possibly unfavorable interaction between the exposed $Ni_{5c}$ with OH* is balanced by the more favorable interactions between Co and OH*.

The free energy change of reaction 2.3 (1.37 eV) is somewhat smaller than that of reaction 2.2 (1.41 eV). We can understand the small reaction free energy change of 2.3 as follows: just like reaction 1.2 for pure NiOOH, this reaction involves the release of a proton from OH* adsorbed on Ni (the breaking of a rather weak metal-OH bond) and the accommodation of O* in the surface. This step (step 1.2 for pure NiOOH in path I) was not the PDS in path I, and the corresponding free energy change was only 1.13 eV in path I. It is therefore not surprising that this step does not hinder path II, so that step 2.2 remains the PDS in the OER on 25% Co-doped NiOOH in path II.

The tactics used in the search procedure for the optimal mechanism for 25% Co-doped NiOOH can be illustrated with the free energy diagrams shown in Figure 5. As both Figures 5A and 5B show, the relative free energy of Config.4 (produced after reactions 1.3 and 2.3) is very close to the ideal level for water splitting after three one-electron transfer steps. The first step of this process should be the deprotonation of a water molecule adsorbed on Co (reaction 2.1 has to be the same as reaction 1.1). The only freedom that remains is to try and swap the second and third reaction steps, which necessarily takes us to the same configuration, from which $O_2$ release represents the next and final step. Figure 5A shows that, compared to the ideal intermediate free energy level for water splitting, the position of the free energy level associated with Config.3 is rather unfavorable in path I. This naturally suggests swapping steps 2 and 3 to see if a more favorable mechanism for the OER can be obtained in this way. Our calculations suggest that this is indeed the case, with the intermediate free energy level associated with Config.3 (2.41 eV) of path II now lying quite close to the ideal value (2.46 eV).

Based on the free energy levels of Configs.2 and 4, and assuming that the extra relaxation possible with the use of a larger surface unit cell does not lead to a significant change in the reaction energies, we can estimate whether the use of the higher Co doping level (50%) could lead to an ever lower overpotential than the value observed for 25% Co doping (0.18 V). Specifically, the lowest overpotential that could be obtained

with path II for 50% Co doped NiOOH is equal to ($G_{config.4}$-$G_{config.2}$)/2q -1.23 V. Using Table 2, we find that the lower bound to the overpotential obtained in this way is 0.225 V. This suggests that increased Co doping is not likely to lead to a further decreased overpotential.

We also explored the reaction energies of the OER on the pure surface under path II, using the LC to check whether this might give rise to a lower overpotential. Figure 4 and Table 2 report the optimized configurations and the reaction energies, respectively. The pure surface shows a different energy profile than the doped one; the PDS is still reaction 2.2, but the associated $\eta$ is 0.51 V rather than 0.18 V. Compared to the $\beta$-NiOOH surface studied with the SC, the first proton release from an adsorbed water molecule in the first reaction, is much more favorable energetically ($\Delta G$ = 1.29 with the LC with respect to $\Delta G$ = 1.70 for reaction 1.1 with the SC). This could be due to the same reasons as discussed earlier for the difference observed for Co-doped NiOOH when varying cell size: the increased stability of Config.2 in the LC could be due to less repulsive electrostatic interactions between the periodic images of the OH*, and it is possible that there are effects of whether or not the $H_2O$ (or $H_2O$-OH) overlayer is commensurate with the size of the surface unit cell (see the previous section).

Under mechanism II for the pure surface, reaction 2.2 involves a second release of a proton from an adsorbed water molecule that interacts with an exposed $Ni_{5c}$ to produce OH*. The high free energy change associated with this reaction, $\Delta G$ = 1.74, may be due to unfavorable interactions between the two adjacent OH*, and in any case we would expect a higher free energy level of Config.3 for NiOOH than for Co-doped NiOOH under path II, because the two OH* both have to adsorb to $Ni_{5c}$ atoms. A Bader charge analysis on the Config. 3, shows different values for Co (0.38) and Ni (1.43), which confirms the stronger metal-OH charge transfer in the formed Co-OH bond and explains the different overpotential values.

As we can see from Figure 5B the cumulative free energy of Config.3 on NiOOH ($\Delta G$ 2.1 + $\Delta G$ 2.2 = 3.03 eV) deviates from the ideal value for splitting water (2.46 eV) by more than 0.5 eV. Table 4 contains the Ni-$OH_2$(OH) distances obtained for the LC for the pure and Co-doped surfaces. The results presented so far lead to the following intermediate conclusions. The lowest overpotential for the OER on NiOOH that we obtained so far is 0.47 V, and on the pure surface the OER proceeds according to mechanism I. Doping the surface layer with 25% Co reduces the overpotential to only 0.18 V, and over the doped surface the OER proceeds according to mechanism II.

### 3.5 Path I on the pure $\beta$-NiOOH surface using the large unit cell

In the following we discuss the OER mechanism on the pure $\beta$-NiOOH using the large cell (LC) according to path I. The OER configurations and the reaction energies are reported in Figure 3 and in Table 1, respectively. As expected and previously anticipated, the $\eta$ for this surface is only 0.28 V, decreasing from 0.47 in the SC to 0.28 V with the LC. Going from the SC to the LC surface we observe not only a large decrease of $\eta$ by 0.19 V, but also a change in PDS from the first to the second step. $\Delta G$ 1.1 involves the same configurations as in the $\beta$-NiOOH surface in the LC according to path II and it has already been discussed in the previous section. A comparison of the free energy profiles in Figure 5A between the $\beta$-NiOOH LC (black line) and SC (orange line) shows clearly that $\Delta G$ 1.1 is smaller with the LC than with the SC, due to the higher stability of Config.2 with the LC than with the SC. In fact, Config.2 decreases in energy relative to Config.1 by 0.41 eV. The increased stability of Config.2 with the LC could be due, once again, to the less repulsive electrostatic interactions between OH* and its periodic images and the better arrangement of the overlayer of the water molecules with the increased size of the surface. $\Delta G$ 1.2 is the free energy change corresponding to the PDS for this mechanism and it is a bit higher with the LC than with the SC, with values of 1.51 and 1.13 eV, respectively. Nevertheless, the cumulative free energy $\Delta G$ 1.1+ $\Delta G$ 1.2 is very similar for the pure surface with the LC and with the SC (2.80 and 2.83 eV, respectively). Moreover, Config.3 is slightly more stable with the LC than with the SC, perhaps due to greater capacity of the larger surface unit cell to accommodate the strain due to the presence of the O-adatom. $\Delta G$ 1.3 is also lower with the LC than with the SC for the same reasons. The main conclusions to draw for the pure surface is that cell size plays a key role mainly due to a greater capacity of the bigger cell to arrange the overlayer of $H_2O$-OH molecules on the surface, increasing both the stability of Config.2 and Config.3. Table 3 presents the different values of the Ni-$OH_2$(OH) distances going from the SC to the LC. Indeed, we have shown that the reorganization of the solvent on the surface affects both the interaction between the adsorbates itself and between the solvent (water molecules) and the surface, which in turn plays a role in the decrease of the overpotential of the OER mechanism. In summary, cell size importantly affects the results of the reaction energies of the OER if the water overlayer is considered, and these effects should probably be addressed in future studies on other systems as well.

### 3.6 Comparison of all scenarios

Starting from the results by Li and Selloni on the pure $\beta$-NiOOH in SC, we explored the effect of doping the $\beta$-NiOOH surface with Co and of unit cell size on the oxidation of water.

For the pure $\beta$-NiOOH the preferential mechanism is path I in agreement with Li and Selloni. Concerning the effect of the size of the surface and in addition to their results, we found that going from SC to LC, the overpotential decreases quite dramatically from 0.47 to 0.28 V by 0.19 V. Further studies which consider also different sizes of the cell in the *y* direction are suggested to investigate the effect of electrostatic interactions and of the commensurate overlayer of the $H_2O$ with the cell on the OER energies.

Concerning the effect of doping the $\beta$-NiOOH surface, we explored two different relative amounts of Co atoms in the exposed layer of the surface: 25% and 50%. When we consider 25% of Co on the topmost layer of the pure surface, we find an overpotential of only 0.18 V with the LC according to path II. On the contrary, doping the pure surface with 50% of Co leads to an increase of the overpotential irrespective of the path considered, up to 0.58 V with the SC.

Our work is in disagreement with the experimental work of Trotochaud et al.[23], who report a small increase of overpotential for the OER on $Ni_yCo_{1-y}O_x$ thin films going from $y = 1.0$ to 0.75. They attribute this decrease to "suppressed in situ formation of the active layered oxyhydrydroxide with increasing Co"[23]. Our work suggests that if the Co-doping could be performed while leaving the oxyhydrydroxide top layer intact, this could instead lead to increased activity of the $Ni_yCo_{1-y}O_x$ catalyst with decreasing y, between *y* equals 1.0 and 0.75. Our results may also be compared with the results of Bajdich et al.[33] for $\beta$-CoOOH and Ni-doped $\beta$-CoOOH. Working from the other end ($y = 0.25$ and 0 are considered), Bajdich et al. find a synergistic effect of Ni and Co but they find that increasing Ni content leads to increased activity for the OER. These results can not be directly compared to ours because they considered a different regime of *y*-values (0.25 and 0). Finally, our results are in disagremeent with some findings and conclusions by Li and Selloni. In particular, in their paper they suggested that while Fe doping NiOx would enhance the OER activity, Co doping would make it slower. They reached this conclusion considering the first proton release as the PDS for pure CoOOH (and not Co-doped NiOx). With our work we demonstrate that, for the Co doped $\beta$-NiOOH, instead the second proton release is the PDS for the most favourable mechanism considered.

## 4 Conclusions

We have explored the OER energetic pathways on the $\beta$-$Ni_yCo_{1-y}OOH$ $(01\bar{1}5)$ surface with *y* varying between 1 (pure $\beta$-NiOOH) and 0.5 (50% Co doped $\beta$-NiOOH), using the DFT + U method. To allow the effect of different doping levels and of the commensurate overlayer of the water to be explored, two cells of different size were used, i.e. the small cell (SC, for $y = 1$ and 0.5) and the large cell (LC, for $y = 1$, and 0.75). Furthermore, the OER was allowed to proceed according to two different mechanisms. In path I, the first deprotonation of an adsorbed water molecule (leading to OH*) was followed by a second deprotonation leading to O*. In path II, after the first deprotonation step the second deprotonation is of a nearby adsorbed water molecule, leading to two nearby OH* molecules adsorbed to the surface.

For the OER on pure $\beta$-NiOOH $(01\bar{1}5)$ we find good agreement of our computed overpotential (0.47 V) with the results of Li and Selloni (0.46 V, Ref.[22]) if the SC is used, as was done in their work. With the use of the SC, the reaction proceeds according to path I, and the PDS is the first deprotonation step. Interestingly we find that the overpotential decreases to 0.28 V if the reaction energies are modeled with the larger cell. In this scenario the reaction still proceeds according to path I, but the PDS is now the second step. The lower overpotential is attributed to the first step becoming more favorable due to decreased Coulomb repulsion between OH* and its periodic images with the use of the larger cell, and altered energetics due to the commensurate overlayer of the water with the differently sized NiOOH surface unit cell, as imposed through the periodic boundary conditions. The lower overpotential can be also attributed to the change in the metal work function affected by the weak adsorbates (OH*) on the surface. These effects lead to uncertainties in the numerical results of the present and previous[22] calculations, and we suggest that the effect of unit cell size be looked at more closely in future theoretical studies on the energies of redox reactions.

For the OER on Co-doped $\beta$-NiOOH $(01\bar{1}5)$ we find the lowest overpotential (0.18 V). This low overpotential is found for 25% Co-doped $\beta$-NiOOH. For this case, the OER proceeds according to path II, and the PDS is the second step in which a second water molecule is deprotonated, leading to two adjacent OH* on the surface, one on the doped Co and one on a nearest neighbour Ni atom. Our result showing that for $y = 0.75$ a lower overpotential is found than for $y = 1.0$ is in agreement with some earlier studies on $Ni_yCo_{1-y}O_x$ surfaces[29–31], and in disagreement with other studies[23]. In particular, our result is at odds with the recent study of Trotochaud et al.[23], who found a slight increase in the overpotential going from $y = 1.0$ to 0.75. However, they attributed the increase in overpotential to a change in structure of the NiOOH with increased Co-doping. Our results suggest that doping the surface with a small amount of Co might lead to increased activity of the $\beta$-NiOOH catalyst if the doping can be carried out in such a way that the structure of $\beta$-NiOOH is preserved. A comparison with experimental works is rather difficult as many factors play a role during an electrochemical experiment. For example, in the article by Smith et al.[66], amorphous metal oxide films are studied containing Fe, Co and Ni, and the best catalyst toward the OER was obtained by $\alpha$-$Fe_{20}Ni_{80}$ compound. With 40% of Co and 60% of Ni, not a visible

improvement in $\eta$ was obtained. A fair comparison with our work would involve lower percentages of Co in the catalyst, which was not explored. Neverthless, the effect of transition metals as additive to NiOx toward the OER remains highly debated. In a recent article by Lyons et al.[18], the authors found that among the three oxides (Fe, Co and Ni), NiOx shows the best performance while FeO shows the poorest. Other experimental studies[67–69] suggest that the effect of Cobalt doping into the nickel hydroxide is to increase the oxygen overpotential, although they claim that the structure of $\beta$-Nickel hydroxide is not affected by Co and that it is difficult to assess the right amount of the Co due to the presence of Co as impurity already in the NiOx electrode.

### 4.1 Acknowledgements

I wish to thank Geert-Jan kroes and Marc C. van Hemert for the useful discussions and important suggestions. I also thank Bernd Ensing, Annabella Selloni, Ye-Fei Li, Michiel Sprik, Marc Koper's group, and Rutger van Santen for useful discussions. This research was funded through the energy programme of the Dutch National Research School Combination Catalysis (NRSC-Catalysis).

## References

1 M. Grätzel, *Nature*, 2001, **414**, 338.
2 J. Rossmeisl, Z.-W. Qu, H. Zhu, G.-J. Kroes and J. Nørskov, *J. of Electoanal. Chem.*, 2007, **607**, 83.
3 A. Valdés, Z.-W. Qu, G.-J. Kroes, J. Rossmeisl and J. Nørskov, *J. Phys. Chem. C*, 2008, **112**, 9872.
4 A. Valdés and G.-J. Kroes, *J. Phys. Chem. C*, 2010, **114**, 1701.
5 I. Man, H. Su, F. Calle-Vallejo, H. A. Hansen, J. I. Martinez, N. G. Inoglu, J. Kitchin, T. F. Jaramillo, J. Nørskov and J. Rossmeisl, *ChemCatChem*, 2011, **3**, 1159.
6 S. Trasatti, *Electrochim. Acta*, 1991, **36**, 225.
7 J. Bockris and T. Otagawa, *J. Electrochem. Soc.*, 1984, **131**, 290.
8 S. Trasatti, *J. Electroanal. Chem.*, 1980, **111**, 125.
9 H. Dau, C. Limberg, T. Reier, M. Risch, S. Roggan and P. Strasser, *ChemCatChem*, 2010, **2**, 724.
10 D. van der Vliet, D. S. Strmcnik, C. Wang, V. R. Stamenkovic, N. M. Markovic and M. T. M. Koper, *J. Electroanal. Chem.*, 2010, **647**, 29.
11 Y. Lee, J. Suntivich, K. J. May, E. E. Perry and S.-H. Yang, *J. Phys. Chem. Lett.*, 2012, **3**, 399.
12 J. Luo, J.-H. Im, M. T. Mayer, M. Schreier, M. K. Nazeeruddin, N.-G. Park, S. D. Tilley, H. J. Fan and M. Grätzel, *Science*, 2014, **345**, 1593.
13 G. Briggs, E. Jones and W. F. K. Wynne-Jones, *Trans. Faraday Soc.*, 1955, **51**, 1433.
14 R. Barnard, C. Randell and F. Tye, *J. Appl. Electrochem.*, 1980, **10**, 109.
15 M. Carpenter and D. Corrigan, *J. Electrochem. Soc.*, 1989, **136**, 1022.
16 M. Oshitani, Y. sasaki and K. Takashima, *Journal of Power Source*, 1984, **12**, 219.
17 B. Klápště, K.Micka, J. Mrha and J. Vondrák, *J. Power Sources*, 1982, **8**, 351.
18 M. E. G. Lyons and M. P. Brandon, *Int. J. Electrochem. Sci.*, 2008, **3**, 1386.
19 P. W. T. Lu and S. Srinivasan, *J. Electrochem. Soc.*, 1978, **125**, 1416.
20 L. Trotochaud, S. Young, J. K. Ranney and S. W. Boettcher, *J. Am. Chem. Soc*, 2014, **136**, 6744.
21 D. A. Corrigan, *J. Electrochem. Soc.*, 1987, **134**, 377.
22 Y. Li and A. Selloni, *ACS Catal.*, 2014, **4**, 1148.
23 L. Trotochaud, J. K. Ranney, K. N. Williams and S. W. Boettcher, *J. Am. Chem. Soc*, 2012, **134**, 17253.
24 L. Trotochaud, T. J. Mills and S. W. Boettcher, *J. Phys. Chem. Lett.*, 2013, **4**, 931.
25 H. Bode, K. Dehmelt and J. Witte, *Electrochim. Acta*, 1966, **11**, 1079.
26 D. Bediako, B. Lassalle-Kaiser, Y. Surendranath, J. Yano, V. Yachandra and D. G. Nocera, *J. Am. Chem. Soc.*, 2012, **134**, 6801.
27 Y. Surendranath, D. A. Lutterman, Y. Liu and D. G. Nocera, *J. Am. Chem. Soc.*, 2012, **134**, 6326.
28 D. A. Lutterman, Y. Surendranath and D. G. Nocera, *J. Am. Chem. Soc. Comm.*, 2009, **131**, 3838.
29 I. Sadiek, A. M. Mohammad, M. E. El-Shakre, M. S. El-Deab and B. E. El-Anadouli, *J. Solid State Electrochem.*, 2013, **17**, 871.
30 X. Liu, J. Huang, X. Wei, C. Yuan, T. Liu, D. Cao, J. Yin and G. Wang, *Journal of Power Sources*, 2013, **240**, 338.
31 P. Liao, J. A. Keith and E. Carter, *J. Am. Chem. Soc.*, 2012, **134**, 13296.
32 R. Subbaraman, D. Tripkovic, K.-C. Chang, D. Strmcnik, A.P.Paulikas, P. Hirunsit, M. Chan, J. Greeley, V. Stamenkovic and N. M. Markovic, *Nature Materials*, 2012, **11**, 550.
33 M. Bajdich, M. García-Mota, A. Vojvodic, J. K. Nand A. T. Bell, *J. Am. Chem. Soc.*, 2013, **135**, 13521.
34 J. Chen and A. Selloni, *J. Phys. Chem. C*, 2013, **117**, 20002.
35 B. C. G. et al., *Impact of Surface Science on Catalysis*, 2000, 51.
36 T. V. W. Janssens, B. S. Clausen, B. Hvolbaek, H. Falsig, C. H. Christensen, T. Bligaard and J. K. Nørskov, *Topics in Catalysis*, 2007, **44**, 15.

37 L.-L. F. G. Yu, Y. Wu, G.-D. Li, H. Li, Y. Sun, T. Asefa, W. Chen and X. Zou, *J. Am. Chem. Soc.*, 2015, **137**, 14023.

38 J.K.Nørskov, J. Rossmeisl, A. Logadottir, L. Lindqvist, J. Kitchin, T. Bligaard and H. Jonsson, *J. Phys. Chem. B*, 2004, **108**, 17886.

39 T. Bligaard, J. K. Nørskov, S. Dahl, J. Matthiensen, C. H. Christensen and J. Sehested, *J. Catal.*, 2004, **224**, 206.

40 J.K.Nørskov, T. Bligaard, A. Logadottir, S. Bahn, L. B. Hansen, M. Bollinger, H. Bengaard, B. Hammer, Z. Sljivancanin, M. Mavrikakis, S. D. Y. Xu and C. J. H. Jacobsen, *J. Catal.*, 2002, **209**, 275.

41 V. Pallasana and M. Neurock, *J. Catal.*, 2000, **191**, 301.

42 Z.-P. Liu and P. Hu, *J. Chem. Phys.*, 2001, **114**, 8244.

43 A. Logadottir, T. H. Rod and J. Nørskov, *J. Catal.*, 2001, **197**, 229.

44 A. Michaelides, Z.-P. Liu, C. J. Zhang, A. Alavi, D. A. King and P. Hu, *J. Am. Chem. Soc.*, 2003, **125**, 3704.

45 J. Dumesic, D. Rudd, L. Aparicio, J. E. Rekoske and A. A. T. no, *The Microkinetics of Heterogeneous Catalysis, Am. Chem. Soc., Washington, DC*, 1993.

46 B. Hammer, L. B. Hansen and J. Nørskov, *Phys. Rev. B*, 1999, **59**, 7413.

47 P. W. Atkins, *In Physical Chemistry 6th ed.*, 1998, **81**, 485.

48 J. P. Perdew, K. Burke and M. Ernzerhof, *Phys. Rev. Lett.*, 1996, **77**, 3865.

49 M. C. Payne, M. P. Teter, D. C. Allan, T. A. Arias and J. D. Joannopoulos, *Rev. Mod. Phys.*, 1992, **64**, 1045.

50 Z. Zou, K. Sayama and H. Arakawa, *Nature*, 2001, **414**, 625.

51 P. Liao and E. Carter, *Chem. Soc. Rev.*, 2013, **42**, 2401.

52 M. García-Mota, M. Bajdich, V. Viswanathan, A. Vojvodic, A. T. Bell and J. K. N, *J. Phys. Chem. C*, 2012, **116**, 21077.

53 A. J. Cohen, P. Mori-Sánchez and W. Yang, *Science*, 2008, **321**, 792.

54 V. Anisimov, J. Zaanen and O. Andersen, *Phys. Rev. B*, 1991, **44**, 943.

55 A. I. Liechtenstein, V. I. Anisimov and J. Zaanen, *Phys. Rev. B*, 1995, **52**, R5467.

56 S. Dudarev, G. Botton, S. Y. Savrasov, C. J. Humphreys and A. Sutton, *Phys. Rev. B*, 1998, **57**, 1505.

57 M. Cococcioni and S. de Gironcoli, *Phys. Rev. B*, 2005, **71**, 035105.

58 P.A.Ignatiev, N. Negulyaev, D. Bazhanov and V. Stepanyuk, *Phys. Rev. B*, 2010, **81**, 235123.

59 V. Y. Kazimirov, M. B. Smirnov, L. Bourgeois, L. Guerlou-Demourgues, L. Servant, A. M. Balagurov, I. Natkaniec, N. R. Khasanova and E. V. Antipov, *Solid State Ionics*, 2010, **181**, 1764.

60 J. D. Head and M. C. Zerner, *Chem. Phys. Lett.*, 1985, **122**, 264.

61 R. L. Doyle, I. J. Godwin, M. P. Brandon and M. E. G. Lyons, *Phys. Chem. Chem. Phys.*, 2013, **15**, 13737.

62 D. Bediako, Y. Surendranath and D. G. Nocera, *J. Am. Chem. Soc.*, 2013, **135**, 3662.

63 R. L. Doyle and M. E. G. Lyons, *J. Electrochem. Soc.*, 2013, **160**, H142.

64 R. L. Doyle and M. E. G. Lyons, *Phys. Chem. Chem. Phys.*, 2013, **15**, 5224.

65 S. Nie, P. J. Feibelman, N. C. Bartelt and K. Thürmer, *Phys. Rev. Lett.*, 2010, **105**, 026102.

66 R. D. L. Smith, M. S. Prévot, R. D. Fagan, S. Trudel and C. P. Berlinguette, *J. Am. Chem. Soc.*, 2013, **135**, 11580.

67 R. D. Armstrong, G. W. D. Briggs and E. A. Charles, *J. Appl. Electrochem.*, 1988, **18**, 215.

68 C. Faure, C. Delmas and P. Willmann, *J. Power Sources*, 1991, **36**, 497.

69 R. S. Jayashree and P. V. Kamath, *J. Electrochem. Soc.*, 2002, **149**, A761.

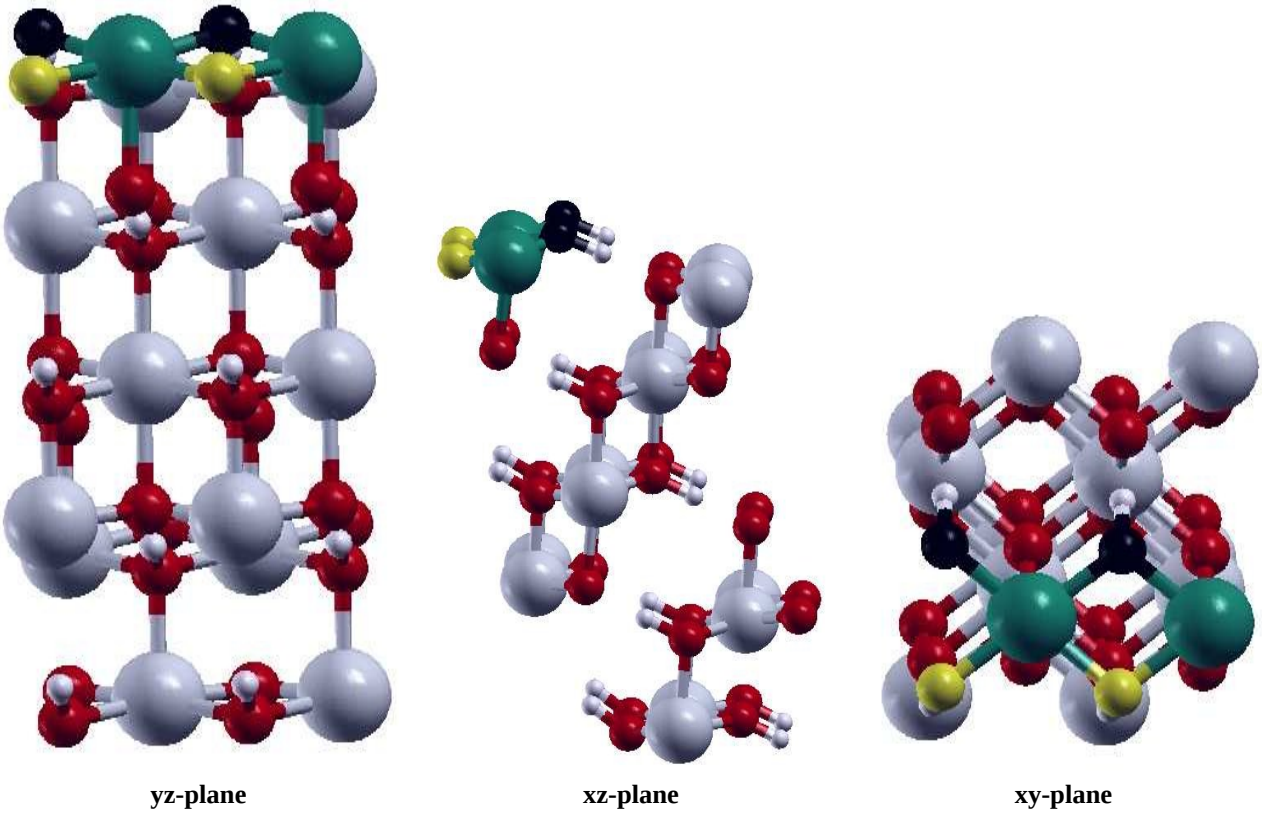


**Fig. 1** Slab of the $\beta$-NiOOH($01\bar{1}5$) surface. From the left: the plane of the paper is the yz, the xz and the xy plane, respectively. Ni, H and O atoms are colored in dark grey, light grey and red, respectively. In green, black and yellow are drawn two $Ni_{5c}$, two $O_{3c}$ and two $O_b$ atoms, respectively

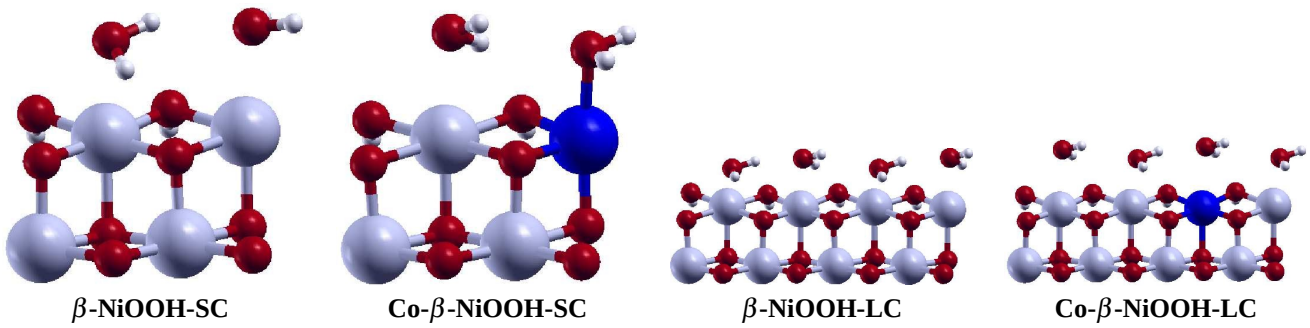


**Fig. 2** Slab surfaces of pure $\beta$-NiOOH and of NiOOH doped with Co. SC and LC stand for small and large cell, respectively. Ni, H, Co and O are drawn in dark grey, light grey, blue and red, respectively

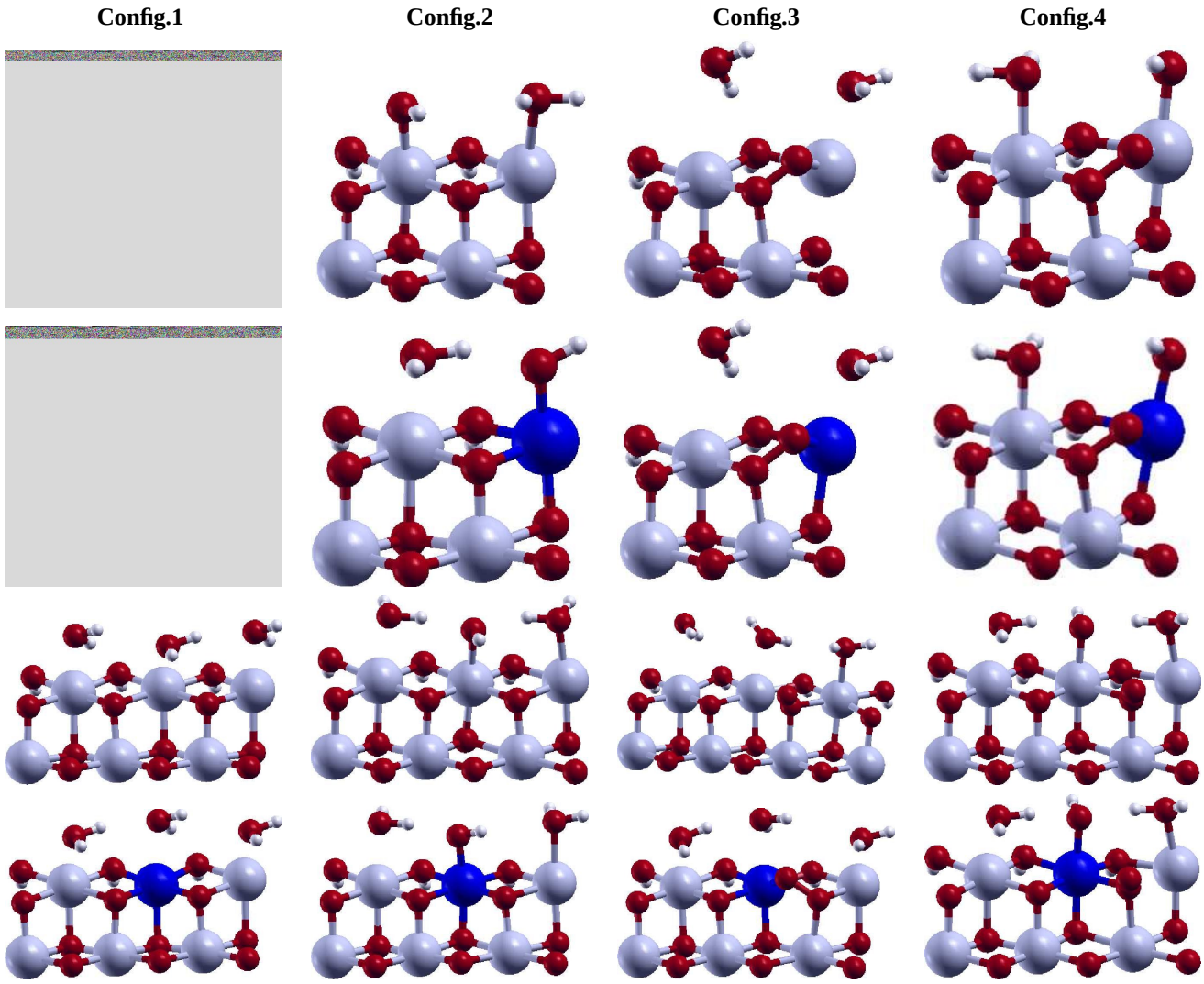


**Fig. 3** Optimized configurations related to the OER according to path I. From the top: the first and the second row represent the pure and the Co-doped $\beta$-NiOOH surfaces studied with the small cell (SC), respectively. The third and the fourth row represent the pure and Co-doped $\beta$-NiOOH surface studied with the large cell (LC), respectively. For clarity for the LC only the three metal atoms involved in the OER are drawn. Ni, H, Co and O are drawn in dark grey, light grey, blue and red, respectively

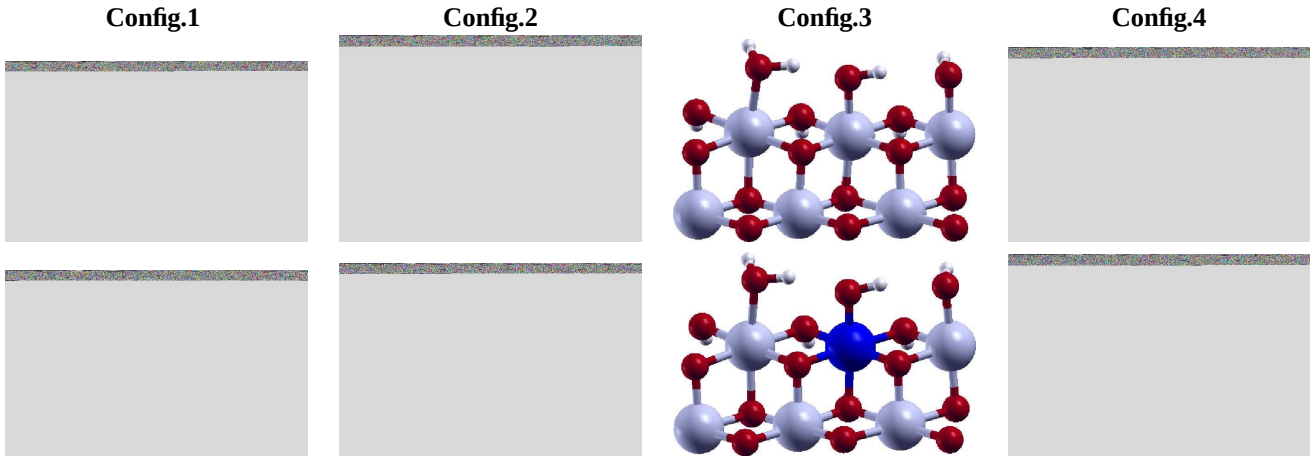


**Fig. 4** Optimized configurations related to the OER according to path II for the pure (top) and the Co-doped $\beta$-NiOOH (bottom) surfaces studied with the large cell (LC). For clarity only the three metal atoms involved in the OER are drawn. Ni, H, Co and O are drawn in dark grey, light grey, blue and red, respectively

**Table 1** Thermodynamic quantities of the four reactions in the OER according to path I for the pure and the Co-doped $\beta$-NiOOH surface studied with the small (SC) and large (LC) cell. All the thermodynamic values are in eV except for the overpotential in V. For brevity, we replaced Conf.1,2,3,4 with 1,2,3,4, respectively. A comparison with Li et al.[22] is provided for the $\beta$-NiOOH surface studied with the SC

| elementary step | $\Delta E$ | $\Delta H_0$ | $\Delta ZPE$ | $-T\Delta S$ | $\Delta G$ | $\eta$ |
|---|---|---|---|---|---|---|
| $\beta$-NiOOH SC path I (Li et al.[22]) | | | | | | |
| $1 + 2\,H_2O(l) \rightarrow 2 + H^+ + e^- + 2\,H_2O(l)$ | 2.06 | 0.04 | −0.21 | −0.20 | 1.69 | 0.46 |
| $2 + 2\,H_2O(l) \rightarrow 3 + H^+ + e^- + H_2O(l)$ | 0.67 | −0.06 | 0.02 | 0.47 | 1.10 | |
| $3 + H_2O(l) \rightarrow 4 + H^+ + e^- + H_2O(l)$ | 1.79 | 0.04 | −0.22 | −0.20 | 1.41 | |
| $4 + H_2O\,(l) \rightarrow 1 + H^+ + e^- + O_2$ | 0.93 | 0.04 | −0.09 | −0.16 | 0.72 | |
| $\beta$-NiOOH SC path I | | | | | | |
| $1 + 2\,H_2O(l) \rightarrow 2 + H^+ + e^- + 2\,H_2O(l)$ | 2.07 | 0.04 | −0.21 | −0.20 | 1.70 | 0.47 |
| $2 + 2\,H_2O(l) \rightarrow 3 + H^+ + e^- + H_2O(l)$ | 0.70 | −0.06 | 0.02 | 0.47 | 1.13 | |
| $3 + H_2O(l) \rightarrow 4 + H^+ + e^- + H_2O(l)$ | 1.79 | 0.04 | −0.22 | −0.20 | 1.41 | |
| $4 + H_2O\,(l) \rightarrow 1 + H^+ + e^- + O_2$ | 0.94 | 0.04 | −0.09 | −0.16 | 0.73 | |
| Co-$\beta$-NiOOH SC path I | | | | | | |
| $1 + 2\,H_2O(l) \rightarrow 2 + H^+ + e^- + 2\,H_2O(l)$ | 1.55 | 0.04 | −0.21 | −0.20 | 1.18 | |
| $2 + 2\,H_2O(l) \rightarrow 3 + H^+ + e^- + H_2O(l)$ | 1.38 | −0.06 | 0.02 | 0.47 | 1.81 | 0.58 |
| $3 + H_2O(l) \rightarrow 4 + H^+ + e^- + H_2O(l)$ | 1.48 | 0.04 | −0.22 | −0.20 | 1.10 | |
| $4 + H_2O\,(l) \rightarrow 1 + H^+ + e^- + O_2$ | 1.13 | 0.04 | −0.09 | −0.16 | 0.92 | |
| $\beta$-NiOOH LC path I | | | | | | |
| $1 + 2\,H_2O(l) \rightarrow 2 + H^+ + e^- + 2\,H_2O(l)$ | 1.66 | 0.04 | −0.21 | −0.20 | 1.29 | |
| $2 + 2\,H_2O(l) \rightarrow 3 + H^+ + e^- + H_2O(l)$ | 1.08 | −0.06 | 0.02 | 0.47 | 1.51 | 0.28 |
| $3 + H_2O(l) \rightarrow 4 + H^+ + e^- + H_2O(l)$ | 1.48 | 0.04 | −0.22 | −0.20 | 1.10 | |
| $4 + H_2O\,(l) \rightarrow 1 + H^+ + e^- + O_2$ | 1.29 | 0.04 | −0.09 | −0.16 | 1.08 | |
| Co-$\beta$-NiOOH LC path I | | | | | | |
| $1 + 2\,H_2O(l) \rightarrow 2 + H^+ + e^- + 2\,H_2O(l)$ | 1.37 | 0.04 | −0.21 | −0.20 | 1.00 | |
| $2 + 2\,H_2O(l) \rightarrow 3 + H^+ + e^- + H_2O(l)$ | 1.36 | −0.06 | 0.02 | 0.47 | 1.76 | 0.53 |
| $3 + H_2O(l) \rightarrow 4 + H^+ + e^- + H_2O(l)$ | 1.37 | 0.04 | −0.22 | −0.20 | 0.99 | |
| $4 + H_2O\,(l) \rightarrow 1 + H^+ + e^- + O_2$ | 1.41 | 0.04 | −0.09 | −0.16 | 1.20 | |

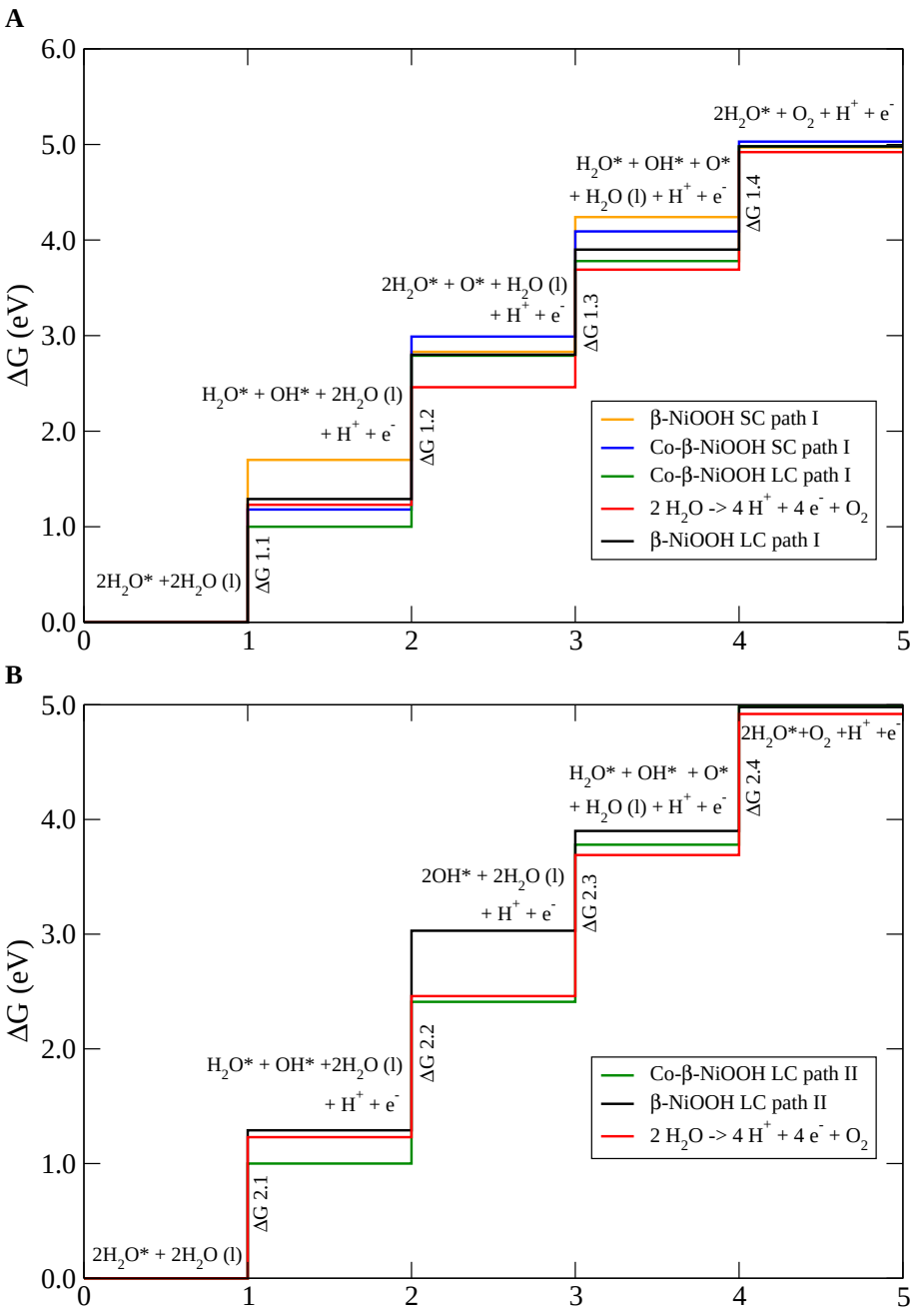


**Fig. 5** Cumulative free energies of the intermediates of the OER according to path I and II on pure and doped surfaces. The ideal cumulative free energies for the water splitting for both paths are reported in red. A: Path I. The free energy values are reported in Table 1. B: Path II. The free energy values are reported in Table 2

**Table 2** Thermodyamic quantities of the four reactions in the OER according to path II for the Co-doped-$\beta$-NiOOH and pure $\beta$-NiOOH surface studied with the large cell (LC) as specified in the Table. All the thermodynamic values are in eV except for the overpotential in V. For brevity, we replaced Conf.1,2,3,4 with 1,2,3,4, respectively

| elementary step | $\Delta E$ | $\Delta H_0$ | $\Delta ZPE$ | $-T\Delta S$ | $\Delta G$ | $\eta$ |
|---|---|---|---|---|---|---|
| Co-$\beta$-NiOOH LC path II | | | | | | |
| $1 + 2\ H_2O(l) \rightarrow 2 + H^+ + e^- + 2\ H_2O(l)$ | 1.37 | 0.04 | −0.21 | −0.20 | 1.00 | |
| $2 + 2\ H_2O(l) \rightarrow 3 + H^+ + e^- + 2\ H_2O(l)$ | 1.79 | 0.04 | −0.22 | −0.20 | 1.41 | 0.18 |
| $3 + 2\ H_2O(l) \rightarrow 4 + H^+ + e^- + H_2O(l)$ | 0.94 | −0.06 | 0.02 | 0.47 | 1.37 | |
| $4 + H_2O(l) \rightarrow 1 + H^+ + e^- + O_2$ | 1.42 | 0.04 | −0.09 | −0.16 | 1.21 | |
| $\beta$-NiOOH LC path II | | | | | | |
| $1 + 2\ H_2O(l) \rightarrow 2 + H^+ + e^- + 2\ H_2O(l)$ | 1.66 | 0.04 | −0.21 | −0.20 | 1.29 | |
| $2 + 2\ H_2O(l) \rightarrow 3 + H^+ + e^- + 2\ H_2O(l)$ | 2.12 | 0.04 | −0.22 | −0.20 | 1.74 | 0.51 |
| $3 + 2\ H_2O(l) \rightarrow 4 + H^+ + e^- + H_2O(l)$ | 0.44 | −0.06 | 0.02 | 0.47 | 0.87 | |
| $4 + H_2O(l) \rightarrow 1 + H^+ + e^- + O_2$ | 1.29 | 0.04 | −0.09 | −0.16 | 1.08 | |

**Table 3** Metal-oxygen and metal-metal distances Å for the surfaces of $\beta$-NiOOH SC, Co-$\beta$-NiOOH SC and Co-$\beta$-NiOOH LC of the four optimized configurations during the OER according to path I. The OER mechanism is shown in Figure 3. The metal can be either Ni or Co depending on the surface

| Atoms | Config.1 | Config.2 | Config.3 | Config.4 |
|---|---|---|---|---|
| | $\beta$-NiOOH SC path I | | | |
| Ni1—$OH_2$ | 2.36 | 2.10 | 2.44 | 1.90 |
| Ni2—$OH_2$ (OH) | 2.37 | 1.87 | 2.24 | 1.95 |
| Ni1—Ni2 | 2.99 | 2.98 | 3.20 | 3.19 |
| | Co-doped-$\beta$-NiOOH SC path I | | | |
| Ni1—$OH_2$ | 2.31 | 2.21 | 3.00 | 1.96 |
| Co2—$OH_2$ (OH) | 2.07 | 1.80 | 2.25 | 1.88 |
| Ni1—Co2 | 3.00 | 2.99 | 3.25 | 3.16 |
| | $\beta$-NiOOH LC path I | | | |
| Ni1—$OH_2$ | 2.25 | 2.22 | 2.87 | 2.27 |
| Ni2—$OH_2$ (OH) | 2.51 | 1.92 | 2.19 | 1.92 |
| Ni3—$OH_2$ | 2.25 | 2.09 | 2.18 | 2.11 |
| Ni1-Ni2 | 2.98 | 2.92 | 2.94 | 2.88 |
| Ni2-Ni3 | 3.00 | 3.04 | 3.27 | 3.25 |
| | Co-doped-$\beta$-NiOOH LC path I | | | |
| Ni1—$OH_2$ | 2.27 | 2.24 | 2.34 | 2.11 |
| Co2—$OH_2$ (OH) | 2.60 | 1.82 | 3.08 | 1.92 |
| Ni3—$OH_2$ | 2.26 | 2.17 | 2.18 | 2.28 |
| Ni1—Co2 | 2.99 | 2.95 | 2.90 | 3.24 |
| Co2-Ni3 | 2.99 | 3.06 | 3.28 | 2.89 |

**Table 4** M-O and M-M distances Å for pure and Co-doped-$\beta$-NiOOH studied with the LC during the four reactions according to path II. The OER mechanism is shown in Figure 4. M can be either Ni or Co depending on the surface

| Atoms | Config.1 | Config.2 | Config.3 | Config.4 |
|---|---|---|---|---|
| | $\beta$-NiOOH LC path II | | | |
| Ni1—$OH_2$ | 2.25 | 2.22 | 2.11 | 2.27 |
| Ni2—$OH_2$ (OH) | 2.51 | 1.92 | 1.85 | 1.92 |
| Ni3—$OH_2$ | 2.25 | 2.09 | 1.88 | 2.11 |
| Ni1–Ni2 | 2.98 | 2.92 | 2.98 | 2.88 |
| Ni2-Ni3 | 3.00 | 3.04 | 2.98 | 3.25 |
| | Co-$\beta$-NiOOH LC path II | | | |
| Ni1—$OH_2$ | 2.27 | 2.24 | 2.15 | 2.11 |
| Co2—$OH_2$ (OH) | 2.60 | 1.82 | 1.79 | 1.92 |
| Ni3—$OH_2$ | 2.26 | 2.17 | 1.89 | 2.28 |
| Ni1—Co2 | 2.99 | 2.95 | 2.99 | 3.24 |
| Co2-Ni3 | 2.99 | 3.06 | 2.99 | 2.89 |